

Pure Moving Electromagnetic Media Consisting of Magneto-chiral Metasurfaces

Toshiyuki Kodama,^{1,*} Toshihiro Nakanishi,² Kei Sawada,^{3,4} and Satoshi Tomita^{1,5,†}

¹*Institute for Excellence in Higher Education, Tohoku University, Sendai 980-8576, Japan*

²*Department of Electronic Science and Engineering, Kyoto University, Kyoto 615-8510, Japan*

³*RIKEN SPring-8 Center, Sayo, Hyogo 679-5148, Japan*

⁴*Cornell High Energy Synchrotron Source, Cornell University, Ithaca, NY 14853, USA*

⁵*Department of Physics, Graduate School of Science, Tohoku University, Sendai 980-8578, Japan*

(Dated: March 7, 2024)

Numerical studies demonstrate that magneto-chiral (MCh) metasurfaces consisting of double Z-type gammadions with perpendicularly magnetized substrate exhibit bianisotropy for microwaves. Effective polarizability tensors of the metasurfaces, extracted from the reflection and transmission coefficients, have components corresponding to non-reciprocal moving-type bianisotropy as well as reciprocal chiral-type bianisotropy and non-reciprocal magneto-optical effects. The combination of the metasurfaces and contraposition MCh metasurfaces cancels the chiral-type bianisotropy and magneto-optical effect, leading to pure moving electromagnetic media. Achieved perfect transmission with phase difference of π realizes an ideal gyrator for arbitrary spatial and polarization modes.

INTRODUCTION

Symmetries relate to physical laws. Noether's theorem says that a system with a continuous symmetry has a conserved quantity, for example, the momentum conservation for spatially uniform systems and the energy conservation for the time-independent systems. Another kind of symmetries is a discrete one, such as spatial inversion and time-reversal symmetry. These symmetries and laws impose restrictions on physical phenomena, and play an essential role in basic and applied physics. Therefore, symmetry breaking would result in emergence of a vast variety of phenomena [1]. In electromagnetism, a breaking of space-inversion and/or time-reversal symmetry allows bianisotropy [2, 3], which represents cross-correlated electromagnetic inductions among electric polarizability, magnetization, and electromagnetic fields in constitutive equations, i.e., magnetoelectric coupling. The bianisotropy is classified into the four categories associated with reciprocity and polarization dependence as follows [4]: a reciprocal chiral-type with polarization plane rotation, a reciprocal omega-type without polarization rotation, a non-reciprocal Tellegen-type with polarization rotation, and a non-reciprocal moving-type without polarization rotation.

While the control of the bianisotropy is a challenge in natural materials with broken symmetry such as multiferroic materials [5–7], man-made structured materials, referred to as metamaterials, are suitable for investigation and control in application of bianisotropy [8–12]. In particular, metasurfaces with two-dimensional planar structures are good playgrounds to embody complex bianisotropic media [13–16]. Here we focus on magneto-chiral (MCh) metasurfaces to realize the fourth type of the bianisotropy classified above, namely the non-reciprocal moving type. The MCh metasurfaces are composed of both chiral meta-atoms with broken space-inversion symmetry and magnetic meta-atoms with broken time-

reversal symmetry. The optical MCh effect is manifested in a transmission coefficient difference, which is dependent on propagation direction but independent of polarization, referred to as directional birefringence [17–33]. The directional birefringence corresponds to the moving-type bianisotropy.

In this work, we numerically calculate transmission and reflection coefficient spectra at microwave frequencies to evaluate effective polarizability tensor [34–36] of MCh metasurfaces. The effective polarizability tensor, extracted from the transmission and reflection coefficients at normal incidence, clearly show optical activity, magneto-optical effect, and electromagnetic moving-medium effect. Furthermore, a composite metasurface consisting of the ordinary and contraposition MCh metasurfaces realizes pure moving electromagnetic media without optical activity and magneto-optical effect. The pure moving media demonstrate the perfect transmission with a phase difference of π depending on propagation direction, bringing about an ideal gyrator [37].

The pure moving electromagnetic media are of great interest in terms of development of functional metasurfaces. A similar story can be found in the development of the well-known negative refractive index metamaterials consisting of double split-ring resonators (SRRs). A single C-shaped SRR shows the omega-type bianisotropy due to electromagnetic interaction in addition to magnetic permeability [38, 39]. This brings about electromagnetic responses not only to magnetic field but also to electric field. An inverse-C-shaped SRR is thus incorporated in the inner circle of the C-shaped SRR, resulting in vanishment of the omega-type electromagnetic interaction but remaining permeability component. In this way, the double SRRs construct pure negative magnetic permeability media, leading to negative refractive index metamaterials. Similarly, the pure moving medium obtained in this study is a key to realize an ideal gyrator for arbitrary spatial and polarization modes. Appli-

cations of the ideal gyrator include an isolator, circulator, non-reciprocal holography [40], two-wavelength lasing [28], and artificial gauge field for light [41]. The pure moving electromagnetic medium is also relevant in basic physics in an analogy with a hypothetical particle called dyon [42], and from the view point of interplay between physics and algebraic geometry in Fresnel-Kummer surfaces [43, 44].

This paper is organized in eight sections. Section II describes the theoretical background of effective polarizability tensor, and explains bianisotropy in four categories. Section III details numerical calculation setup. Section IV devotes to calculation results of microwave transmission and reflection coefficient spectra of uniaxial bianisotropic MCh metasurfaces consisting of double Z-type gammadion [45] with perpendicularly magnetized substrate. The extracted effective polarizability tensors of chiral and MCh metasurfaces are illustrated in Sections V and VI, respectively. Section VII presents pure moving electromagnetic medium by introducing contra-position MCh metasurfaces with the inverse chirality and converse magnetization of the ordinary MCh metasurfaces. The pure moving medium brings about perfect transmission and phase difference of π . Section VIII concludes the paper.

THEORETICAL BACKGROUND

Effective polarizability tensor

The electromagnetic properties of a metasurface, which interacts with normally incident plane waves propagating in the $+z$ direction, can be fully characterized by a following effective polarizability tensor $\hat{\alpha}_{ij}$ defined as

$$\begin{pmatrix} P_x \\ P_y \\ M_x \\ M_y \end{pmatrix} = \begin{pmatrix} \hat{\alpha}_{xx}^{ee} & \hat{\alpha}_{xy}^{ee} & \hat{\alpha}_{xx}^{em} & \hat{\alpha}_{xy}^{em} \\ \hat{\alpha}_{yx}^{ee} & \hat{\alpha}_{yy}^{ee} & \hat{\alpha}_{yx}^{em} & \hat{\alpha}_{yy}^{em} \\ \hat{\alpha}_{xx}^{me} & \hat{\alpha}_{xy}^{me} & \hat{\alpha}_{xx}^{mm} & \hat{\alpha}_{xy}^{mm} \\ \hat{\alpha}_{yx}^{me} & \hat{\alpha}_{yy}^{me} & \hat{\alpha}_{yx}^{mm} & \hat{\alpha}_{yy}^{mm} \end{pmatrix} \begin{pmatrix} E_x^{\text{inc}} \\ E_y^{\text{inc}} \\ H_x^{\text{inc}} \\ H_y^{\text{inc}} \end{pmatrix}, \quad (1)$$

where the superscript e and m in $\hat{\alpha}_{ij}$ are assigned to electric and magnetic stimulus/responses, respectively. The subscript $i = x, y$ ($j = x, y$) in $\hat{\alpha}$ represents the polarization direction of the output (input) waves. The i components ($i = x, y$) of induced electric moment per a unit area, induced magnetic moment per a unit area, incident electric field, and incident magnetic field, are represented respectively by P_i , M_i , E_i^{inc} , and H_i^{inc} [3]. In this way, $\hat{\alpha}_{xy}^{\text{em}}$, for example, represents an effective polarizability tensor element, where a magnetic field in the y direction induces an electric dipole moment in the x direction. General metasurfaces with anisotropic magneto-electric interactions are referred to as bianisotropic metasurfaces.

Here we write the plane waves to be, $E, H \propto e^{j(-\vec{k} \cdot \vec{r} + \omega t)}$, where $j = \sqrt{-1}$ is an imaginary unit. In

this notation, the effective polarizability tensor components can be expressed in a non-dimensional manner to be

$$\alpha_{xx}^{\text{ee}} \omega Z_0 = \frac{j}{2} (t_{xx}^+ + t_{xx}^- + r_{xx}^+ + r_{xx}^- - 2), \quad (2)$$

$$\alpha_{yy}^{\text{mm}} \omega Z_0^{-1} = \frac{j}{2} (t_{xx}^+ + t_{xx}^- - r_{xx}^+ - r_{xx}^- - 2), \quad (3)$$

$$\alpha_{xy}^{\text{em}} \omega = \frac{j}{2} (t_{xx}^+ - t_{xx}^- + r_{xx}^+ - r_{xx}^-), \quad (4)$$

$$\alpha_{yx}^{\text{me}} \omega = \frac{j}{2} (t_{xx}^+ - t_{xx}^- - r_{xx}^+ + r_{xx}^-), \quad (5)$$

$$\alpha_{yx}^{\text{ee}} \omega Z_0 = \frac{j}{2} (t_{yx}^+ + t_{yx}^- + r_{yx}^+ + r_{yx}^-), \quad (6)$$

$$\alpha_{xy}^{\text{mm}} \omega Z_0^{-1} = -\frac{j}{2} (t_{yx}^+ + t_{yx}^- - r_{yx}^+ - r_{yx}^-), \quad (7)$$

$$\alpha_{yy}^{\text{em}} \omega = \frac{j}{2} (t_{yx}^+ - t_{yx}^- + r_{yx}^+ - r_{yx}^-), \quad (8)$$

$$\alpha_{xx}^{\text{me}} \omega = -\frac{j}{2} (t_{yx}^+ - t_{yx}^- - r_{yx}^+ + r_{yx}^-), \quad (9)$$

with transmission coefficients t_{ij}^{\pm} and reflection coefficients r_{ij}^{\pm} , where the superscript \pm represents the sign of z component of the wavevector [36]. A wave impedance of a vacuum is represented by Z_0 . The above components are derived from the transmission and reflection coefficients for x -polarized incident waves, i.e. $t_{ix}^{\pm}, r_{ix}^{\pm}$ ($i = x, y$). The effective polarizabilities given by Eqs. (2) to (5) are related to polarization-maintaining interaction, while those given by Eqs. (6) to (9) are related to interaction involving polarization conversion from x -polarized waves to y -polarized waves. The remaining components can be calculated from the transmission and reflection coefficients for the y -polarized incident waves, i.e. $t_{iy}^{\pm}, r_{iy}^{\pm}$ ($i = x, y$). Suppose a uniaxial metasurface with z -axis rotational symmetry. The following relations hold: $t_{xx}^{\pm} = t_{yy}^{\pm}$, $r_{xx}^{\pm} = r_{yy}^{\pm}$, $t_{xy}^{\pm} = -t_{yx}^{\pm}$, $r_{xy}^{\pm} = -r_{yx}^{\pm}$, which yield $\hat{\alpha}_{xx}^{\text{ee}} = \hat{\alpha}_{yy}^{\text{ee}}$, $\hat{\alpha}_{xx}^{\text{mm}} = \hat{\alpha}_{yy}^{\text{mm}}$, $\hat{\alpha}_{xy}^{\text{em}} = -\hat{\alpha}_{yx}^{\text{em}}$, $\hat{\alpha}_{yx}^{\text{me}} = -\hat{\alpha}_{xy}^{\text{me}}$, $\hat{\alpha}_{yx}^{\text{ee}} = -\hat{\alpha}_{xy}^{\text{ee}}$, $\hat{\alpha}_{xy}^{\text{mm}} = -\hat{\alpha}_{yx}^{\text{mm}}$, $\hat{\alpha}_{xy}^{\text{em}} = \hat{\alpha}_{yx}^{\text{em}}$, $\hat{\alpha}_{xx}^{\text{me}} = \hat{\alpha}_{yy}^{\text{me}}$. As a result, the uniaxial metasurface is fully characterized by the components of the effective polarizability tensor given by Eq. (2) to Eq. (9). In this paper, we evaluate these effective polarizabilities using transmission and reflection coefficients from numerically calculated S parameters of the MCh metasurfaces.

Classification of bianisotropic metasurfaces

Reciprocity in the bianisotropic metasurfaces would require the following relations[3]:

$$\hat{\alpha}_{xx}^{\text{em}} = -\hat{\alpha}_{xx}^{\text{me}}, \hat{\alpha}_{yy}^{\text{em}} = -\hat{\alpha}_{yy}^{\text{me}}, \hat{\alpha}_{xy}^{\text{em}} = -\hat{\alpha}_{yx}^{\text{me}}, \hat{\alpha}_{yx}^{\text{em}} = -\hat{\alpha}_{xy}^{\text{me}}. \quad (10)$$

Uniaxial metasurfaces with magneto-electric interactions can be classified into four categories in terms of non-reciprocity and polarization rotation as shown in Table

TABLE I. Classification of bianisotropic metasurfaces

	Reciprocal	Non-reciprocal
With polarization rotation	Chiral with $\tilde{t}_{yx}^+ \neq \tilde{t}_{yx}^-$	Tellegen with $\tilde{r}_{yx}^+ \neq \tilde{r}_{yx}^-$
Without polarization rotation	Omega with $\tilde{r}_{xx}^+ \neq \tilde{r}_{xx}^-$	Moving with $\tilde{t}_{xx}^+ \neq \tilde{t}_{xx}^-$

I[4]. In the following, we briefly explain each category.

A reciprocal metasurface with polarization rotation is referred to as a chiral metasurface. In the chiral metasurface, the uniaxial structure and the reciprocity require transmission coefficients \tilde{t}_{yx}^\pm to be

$$\tilde{t}_{yx}^+ - \tilde{t}_{yx}^- = -j\omega(\hat{\alpha}_{yy}^{\text{em}} - \hat{\alpha}_{xx}^{\text{me}}) = -j\omega(\hat{\alpha}_{yy}^{\text{em}} - \hat{\alpha}_{yy}^{\text{me}}) \neq 0. \quad (11)$$

Equation (11) implies an optical activity, in which the transmission coefficients depend on propagation direction, and the polarization rotation is reversed for opposite propagating waves. Note that magnetized media or media under magnetic fields could show similar polarization rotation in transmission, known as the Faraday effects, with $\tilde{t}_{yx}^+ \propto \hat{\alpha}_{yx}^{\text{ee}}$ or $\tilde{t}_{yx}^+ \propto \hat{\alpha}_{yx}^{\text{mm}}$. However, these non-reciprocal magneto-optical effects do not show propagation direction dependence with respect to polarization rotation direction.

The reflection coefficients with polarization rotation, \tilde{r}_{yx}^\pm , lead to

$$\tilde{r}_{yx}^+ - \tilde{r}_{yx}^- = -j\omega(\hat{\alpha}_{yy}^{\text{em}} + \hat{\alpha}_{xx}^{\text{me}}) = -j\omega(\hat{\alpha}_{yy}^{\text{em}} + \hat{\alpha}_{yy}^{\text{me}}). \quad (12)$$

Equation (12) becomes zero for the reciprocal chiral metasurfaces due to $\hat{\alpha}_{yy}^{\text{em}} = -\hat{\alpha}_{yy}^{\text{me}}$ as in Eq. (10), but could be non-zero for non-reciprocal ones. When we compare reflection coefficients between x -polarized and y -polarized waves propagating in $+z$ direction without magneto-optical effects, we obtain $\tilde{r}_{yx}^+ = -j\omega(\hat{\alpha}_{yy}^{\text{em}} + \hat{\alpha}_{xx}^{\text{me}}) = -\tilde{r}_{xy}^+$. The non-reciprocal metasurface with polarization rotation in reflection is referred to as a Tellegen metasurface, named after Bernard Tellegen [46]. The Tellegen metasurface shows polarization rotation in the same direction independent of polarization directions [4]. Because this is a non-reciprocal phenomenon with broken time-reversal symmetry, Tellegen metasurface seems to be similar to magneto-optical media mentioned in the above. However, the Tellegen metasurface does not show any polarization rotations in the transmission.

The reflection coefficients without polarization rotation have the following relation,

$$\tilde{r}_{xx}^+ - \tilde{r}_{xx}^- = -j\omega(\hat{\alpha}_{xy}^{\text{em}} - \hat{\alpha}_{yx}^{\text{me}}). \quad (13)$$

Equation (13) could become non-zero even in reciprocal metasurfaces due to $\hat{\alpha}_{xy}^{\text{em}} = -\hat{\alpha}_{yx}^{\text{me}}$ as in Eq. (10). In this case, reflection coefficients without polarization rotation depend on incident direction [12], and the metasurface

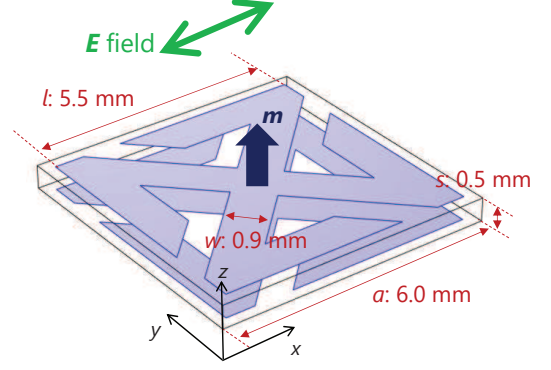


FIG. 1. A unit cell of calculated MCh metasurface consisting of 5.5 mm \times 5.5 mm Z-type gammadions on the both sides of a 0.5 mm-thick substrate. The substrate is magnetized in the $+z$ direction. Electric field of the incident microwave is polarized along x direction.

with $\tilde{r}_{xx}^+ \neq \tilde{r}_{xx}^-$ is referred to as an omega metasurface, which is typically observed with omega-shaped metallic structures, such as SRRs.

The transmission coefficients without polarization rotation have the following relation,

$$\tilde{t}_{xx}^+ - \tilde{t}_{xx}^- = -j\omega(\hat{\alpha}_{xy}^{\text{em}} + \hat{\alpha}_{yx}^{\text{me}}), \quad (14)$$

which is always zero for reciprocal metasurfaces owing to $\hat{\alpha}_{xy}^{\text{em}} = -\hat{\alpha}_{yx}^{\text{me}}$ as in Eq. (10), and could be non-zero for non-reciprocal metasurfaces. The symmetric off-diagonal parts in magneto-electric interactions, i.e., $\hat{\alpha}_{xy}^{\text{em}} = \hat{\alpha}_{yx}^{\text{me}} \neq 0$ causes directional-dependent transmission coefficients, which correspond to the MCh effect. The metasurface with $\tilde{t}_{xx}^+ \neq \tilde{t}_{xx}^-$ is called a moving metasurface, which shows electromagnetic responses similar to that of a medium in move with a constant velocity.

NUMERICAL SIMULATION SETUP

Figure 1 illustrates a unit cell of the uniaxial metasurface in this study. The metasurface consists of Z-type gammadions with $l = 5.5$ mm on the both sides of a substrate with $s = 0.5$ mm. The double Z-type gammadions are identical to those studied in Ref. [45]. The gammadions are made of perfect electric conductor with $w = 0.9$ mm, and in the unit cell with $a = 6.0$ mm, which is repeated in the x and y directions by a periodic boundary condition. The substrate is magnetized in the $+z$ direction. The relative electric permittivity of the substrate is constant ($\epsilon_r = 3.3$), while the relative magnetic permeability expressed by a tensor μ_r is varied. The permeability tensor μ_r for lossless media is described by

$$\mu_r = \begin{bmatrix} 1 & jm & 0 \\ -jm & 1 & 0 \\ 0 & 0 & 1 \end{bmatrix}, \quad (15)$$

where a parameter denoted by m is related to magnetization of the substrate. The substrate is non-magnetic when $m = 0$. On the other hand, $m > 0$ correspond to magnetic substrates magnetized in the $+z$ direction indicated as a navy arrow in Fig. 1. Non-zero m causes non-zero off-diagonal components in μ_r , resulting in magneto-optical effects.

The S -parameters for microwave transmission and reflection are numerically calculated using RF module of COMSOL Multiphysics. The metasurface in the x - y plane is placed at $z = 0$ in a vacuum ranging from $z = +15$ mm to $z = -15$ mm. Ports 1 and 3 are set at $z = +15$ mm, while ports 2 and 4 are set at $z = -15$ mm. The calculation space is terminated by 15 mm-long perfect matching layers at the both ends of the vacuum. The microwaves in a frequency range between 4 and 16 GHz propagate in $-z$ direction from the port 1 to the metasurface. Incident microwave is linearly polarized along x -direction as indicated by a green arrow in Fig. 1. We numerically calculate S_{11} detected by the port 1 corresponding to reflection with x -polarization, S_{21} detected by the port 2 corresponding to transmission with x -polarization, S_{31} detected by the port 3 corresponding to reflection with y -polarization, and S_{41} detected by the port 4 corresponding to transmission with y -polarization.

The S -parameters S_{11} , S_{21} , S_{31} , and S_{41} are converted to reflection and transmission coefficients of the metasurface by using $r_{xx}^- = S_{11}e^{jk_0d}$, $t_{xx}^- = S_{21}e^{jk_0d}$, $r_{yx}^- = S_{31}e^{jk_0d}$, and $t_{yx}^- = S_{41}e^{jk_0d}$, where k_0 is the wavenumber in a vacuum. In the same fashion, reflection and transmission coefficients for incident waves propagating in the $+z$ direction can be calculated. By using these coefficients, we obtain each component of the effective polarizability tensor.

TRANSMISSION AND REFLECTION SPECTRA OF CHIRAL AND MAGNETOCHIRAL METASURFACES

Figure 2(a) shows calculated transmission and reflection amplitude spectra of $|r_{xx}^-|$ (black), $|t_{xx}^-|$ (red), $|r_{yx}^-|$ (blue), and $|t_{yx}^-|$ (green) between 4 to 16 GHz for a chiral metasurface with $m = 0$. Note that $|r_{yx}^-|$ is almost zero at this frequency region. In $|r_{xx}^-|$ spectrum, a sharp dip appears at 7.5 GHz, while a broad dip appears at 13.1 GHz. At each frequency, $|t_{xx}^-|$ spectrum exhibits dispersion-type features. These are caused by resonances by the double Z-type gammadions. The resonance in the gammadion structures results in polarization rotation of linearly polarized microwave, i.e., optical activity. Indeed, in Fig. 2(a), $|t_{yx}^-|$ spectrum shows a sharp peak at 7.5 GHz, and a broad peak at 13.1 GHz, demonstrating the optical activity by the double Z-type gammadions [45].

Figure 2(b) shows calculated spectra of $|r_{xx}^-|$ (black),

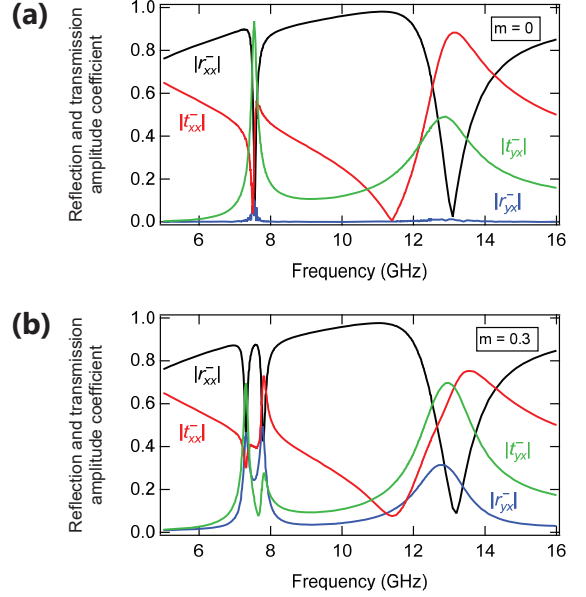


FIG. 2. Calculated spectra of $|r_{xx}^-|$ (black), $|t_{xx}^-|$ (red), $|r_{yx}^-|$ (blue), and $|t_{yx}^-|$ (green) between 4 to 16 GHz with (a) $m = 0$ and (b) $m = 0.3$.

$|t_{xx}^-|$ (red), $|r_{yx}^-|$ (blue), and $|t_{yx}^-|$ (green) between 4 to 16 GHz for an MCh metasurface with $m = 0.3$. In contrast to Fig. 2(a), $|r_{yx}^-|$ in Fig. 2(b) shows peaks at approximately 7.5 and 13.1 GHz. In all spectra, the resonant mode around 7.5 GHz is split into two at 7.3 and 7.8 GHz. By introducing perpendicular magnetization in the substrate, MCh effects is induced. To verify MCh effects, we observe transmission phase spectra.

Figure 3(a) shows phase spectra of the chiral metasurface with $m = 0$. The phase spectrum $(\arg t_{xx}^-)/\pi$ (black solid) corresponds to a transmission phase spectrum of $-z$ direction propagation while $(\arg t_{xx}^+)/\pi$ (red dashed) to that of $+z$ direction propagation. In Fig. 3(a), although the phase shift is observed at 7.5 GHz and 13.1 GHz corresponding to resonance in the gammadion structures, $(\arg t_{xx}^-)/\pi$ and $(\arg t_{xx}^+)/\pi$ are identical. However, by introducing magnetization with $m = 0.3$, a phase difference appears as in Fig. 3(b). In Fig. 3(b), $(\arg t_{xx}^-)/\pi$ (black solid) is different from $(\arg t_{xx}^+)/\pi$ (red dashed) in regions from 7 to 8 GHz and from 10 to 13 GHz. Figure 3(c) represents directional phase difference spectra $(\arg t_{xx}^- - \arg t_{xx}^+)/\pi$ for $m = 0$ (black) and $m = 0.3$ (red). While no phase difference is observed with $m = 0$, a significant phase difference is observed with $m = 0.3$. The phase difference clearly indicates that the MCh effect is induced in the double Z-type gammadions with perpendicular magnetization.

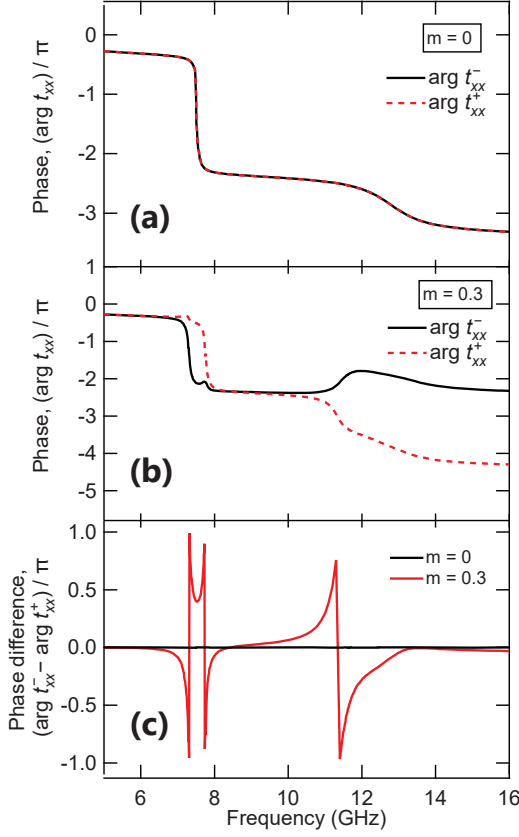


FIG. 3. Calculated spectra of $(\arg t_{xx}^-)/\pi$ (black solid) and $(\arg t_{xx}^+)/\pi$ (red dashed) for (a) $m = 0$ and (b) $m = 0.3$ between 4 to 16 GHz. (c) $(\arg t_{xx}^- - \arg t_{xx}^+)/\pi$ spectra for $m = 0$ (black) and $m = 0.3$ (red).

EFFECTIVE POLARIZABILITY TENSOR OF CHIRAL METASURFACES

Figure 4 shows frequency spectra of extracted effective polarizabilities of the chiral metasurface with $m = 0$. Solid and dotted lines correspond to the real and imaginary parts, respectively. In Fig. 4(a), $\alpha_{xx}^{ee}\omega Z_0$ (red) corresponds to the diagonal part of electric susceptibility while $\alpha_{yy}^{mm}\omega Z_0^{-1}$ (blue) corresponds to the diagonal part of magnetic susceptibility. The $\alpha_{xx}^{ee}\omega Z_0$ spectrum representing electric dipole oscillation exhibits a sharp resonance feature at 7.5 GHz and broad feature at 13 GHz. The $\alpha_{yy}^{mm}\omega Z_0^{-1}$ spectrum representing magnetic dipole oscillation exhibits a sharp resonance at 7.5 GHz and very broad feature at 13 GHz. Figure 4(a) highlights that, although electric dipole and magnetic dipole coexist both at 7.5 and 13 GHz, electric dipole oscillation is dominant at 13 GHz.

Figure 4(b) represents the off-diagonal part of electric susceptibility, $\alpha_{yx}^{ee}\omega Z_0$ (black), and the off-diagonal part of magnetic susceptibility, $\alpha_{xy}^{mm}\omega Z_0^{-1}$ (pink). Figure 4(b) indicates that magneto-optical effects does not exist in the double Z-type gammadion with a non-magnetic

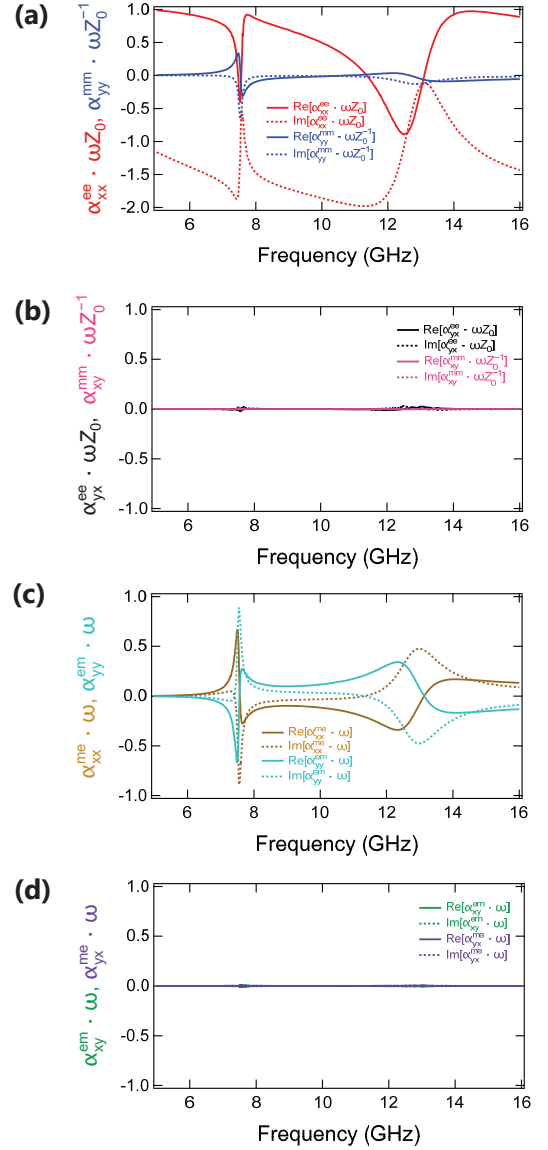


FIG. 4. Effective polarizabilities of chiral metasurfaces with $m = 0$ evaluated from numerical simulation. Frequency versus extracted (a) $\alpha_{xx}^{ee}\omega Z_0$ (red) and $\alpha_{yy}^{mm}\omega Z_0^{-1}$ (blue), (b) $\alpha_{yx}^{ee}\omega Z_0$ (black) and $\alpha_{xy}^{mm}\omega Z_0^{-1}$ (pink), (c) $\alpha_{xx}^{me}\omega$ (gold) and $\alpha_{yy}^{em}\omega$ (cyan), (d) $\alpha_{xy}^{em}\omega$ (green) and $\alpha_{yx}^{me}\omega$ (purple). Solid and dotted lines correspond to real and imaginary parts, respectively.

substrate. In Fig. 4(d), $\alpha_{xy}^{em}\omega$ (green) and $\alpha_{yx}^{me}\omega$ (purple) correspond to omega or moving components. Figure 4(d) demonstrates that moving and omega components are absent.

In Fig. 4(c), $\alpha_{xx}^{me}\omega$ (gold) and $\alpha_{yy}^{em}\omega$ (cyan) correspond to chiral or Tellegen components. The effective polarizabilities $\alpha_{xx}^{me}\omega$ and $\alpha_{yy}^{em}\omega$ show resonant features at 7.5 and 13 GHz. We notice here $\alpha_{xx}^{me} = -\alpha_{yy}^{em}$. Given $\alpha_{yy}^{em} = \alpha_{xx}^{em}$ due to the rotational symmetry, $\alpha_{xx}^{me} = -\alpha_{xx}^{em}$ is satisfied as Eq. (10); this is the hallmark of the re-

reciprocal chiral-type bianisotropy. In this way, Fig. 4(c) demonstrates that the double Z-type gammadion with the non-magnetic substrate shows polarization rotation by reciprocal chiral-type bianisotropy. This is consistent with the fact that $|r_{yx}^-| \sim 0$ is observed in Fig. 2(a).

EFFECTIVE POLARIZABILITY TENSOR OF MAGNETOCHIRAL METASURFACE

Figure 5 shows extracted effective polarizabilities of the MCh metasurface with $m = 0.3$. Solid and dotted lines correspond respectively to real and imaginary parts. Figure 5(a) shows that the resonant mode originally at 7.5 GHz with $m = 0$ is split into two modes at 7.3 and 7.8 GHz with $m = 0.3$. Figure 5(c) represents that the double Z-type gammadion with perpendicularly magnetized substrate exhibits reciprocal chiral-type bianisotropy, i.e., optical activity at 7.3, 7.8 and 13 GHz, which is similar to Fig. 4(c).

Contrastingly, by introducing perpendicular magnetization in the substrate, Figs. 5(b) and 5(d) are much different from Fig. 4(b) and Fig. 4(d). In Fig. 5(b), the off-diagonal part of electric susceptibility $\alpha_{yx}^{ee}\omega Z_0$ (black) and the off-diagonal part of magnetic susceptibility $\alpha_{xy}^{mm}\omega Z_0^{-1}$ (pink) show resonant features at approximately 7.5 and 13 GHz, indicating that magneto-optical effects emerge due to the time-reversal symmetry breaking. Moreover, Fig. 5(d) shows non-zero $\alpha_{xy}^{em}\omega$ (green) and $\alpha_{yx}^{me}\omega$ (purple), which correspond to moving or omega-type bianisotropy. Given that $\alpha_{xy}^{em}\omega = \alpha_{yx}^{me}\omega$ is satisfied in Fig. 5(d), Eq. (10) indicates that the resonant features at 7.5 and 13 GHz are originated from the non-reciprocal moving-type bianisotropy. Effective polarizability tensor analysis shown in Fig. 5 reveals that the double Z-type gammadion with the perpendicularly magnetized substrate exhibits non-reciprocal moving-type bianisotropy without polarization rotation as well as optical activity and magneto-optical effect involving polarization rotation. Note here that the non-reciprocal moving-type bianisotropy observed in Fig. 5(d) includes cascaded MCh effect [27], which is a combination between optical activity and magneto-optical effect.

PURE MOVING MEDIUM WITH COMPOSITE MAGNETOCHIRAL METASURFACE

To obtain pure moving metasurface, we propose a composite metasurface that combines the ordinary MCh metasurfaces studied in the above with contraposition MCh metasurfaces. Figure 6(a) shows a unit cell of the combined metasurfaces consisting of ordinary MCh metasurfaces and contraposition MCh metasurfaces, which have double inverse-Z-type gammadions and oppositely magnetized substrates. Optical activity is cancelled by

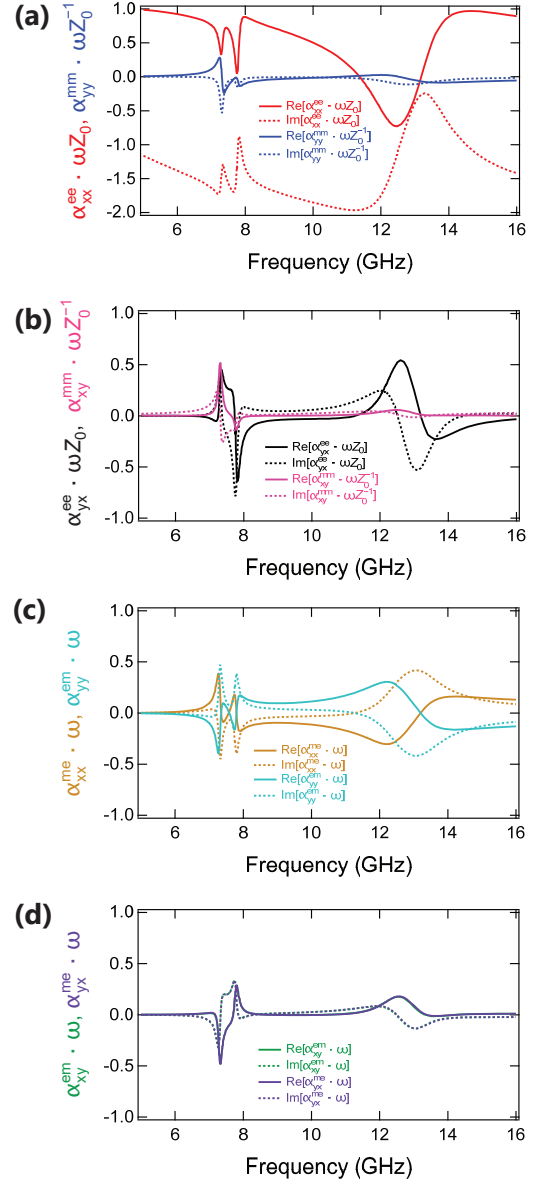


FIG. 5. Effective polarizabilities of magnetochiral metasurfaces with $m = 0.3$ evaluated from numerical simulation. Frequency versus extracted (a) $\alpha_{xx}^{ee}\omega Z_0$ (red) and $\alpha_{yy}^{mm}\omega Z_0^{-1}$ (blue), (b) $\alpha_{yx}^{ee}\omega Z_0$ (black) and $\alpha_{xy}^{mm}\omega Z_0^{-1}$ (pink), (c) $\alpha_{xx}^{me}\omega$ (gold) and $\alpha_{yy}^{em}\omega$ (cyan), (d) $\alpha_{xy}^{em}\omega$ (green) and $\alpha_{yx}^{me}\omega$ (purple). Solid and dotted lines correspond to real and imaginary parts, respectively.

double inverse-Z-type gammadion with inverse chirality, similar to racemate of chiral chemical compounds. Additionally, as shown in Fig. 6(a), the contraposition metasurfaces have inverse magnetization in the $-z$ direction while the ordinary metasurfaces have magnetization in the $+z$ direction. Therefore magneto-optical effect vanishes due to anti-parallel magnetization, similar to anti-ferromagnet. Nevertheless, because MCh effect is an odd function of chirality and magnetization direction,

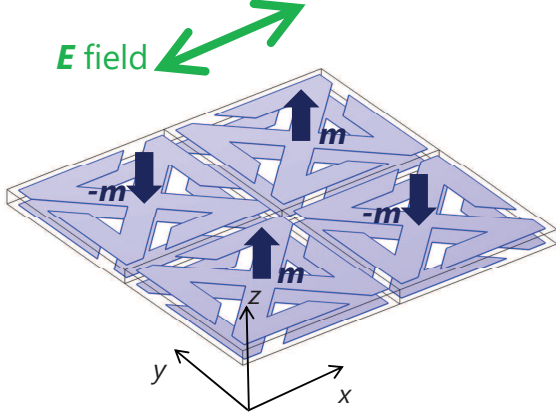


FIG. 6. A unit cell including ordinary and contraposition MCh metasurfaces. Electric field of the incident microwave is polarized along the x direction.

the contraposition metasurfaces consisting of the double inverse-Z-type gammadions with the converse magnetization in the $-z$ direction has the identical sign of MCh effect with the ordinary metasurfaces consisting of double Z-type gammadions with magnetization in the $+z$ direction. In this way, combination between ordinary and contraposition MCh metasurfaces is anticipated to exhibit only moving bianisotropy.

Figure 7(a) highlights calculated spectra of $|r_{xx}^-|$ (black), $|t_{xx}^-|$ (red), $|r_{yx}^-|$ (blue), and $|t_{yx}^-|$ (green) in a frequency range between 4 to 16 GHz of the composite MCh metasurface with $m = \pm 0.3$. In Fig. 7(a), $|r_{xx}^-|$ (black) and $|t_{xx}^-|$ (red) show resonant features at 7.2, 7.8, 12.0, and 13.2 GHz. Moreover, $|r_{yx}^-|$ (blue) and $|t_{yx}^-|$ (green) accompanied by polarization rotation are almost zero, indicating that chiral-type bianisotropy and magneto-optical effect with polarization rotation are no longer functioning in the composite metasurface. However, the moving-type bianisotropy is expected to be survived as shown in Figs. 7(b) and 7(c). Figure 7(b) shows transmission phase spectra of $(\arg t_{xx}^-)/\pi$ (black solid) and $(\arg t_{xx}^+)/\pi$ (red dashed) of the composite metasurfaces. Phase differences are observed at approximately 7.5 GHz and 12 GHz. The directional phase difference spectrum, $(\arg t_{xx}^- - \arg t_{xx}^+)/\pi$, plotted in Fig. 7(c) clearly shows the MCh effect with the moving-type bianisotropy at approximately 7.5 GHz and 12 GHz.

Figure 8 shows extracted (a) $\alpha_{xx}^{\text{ee}}\omega Z_0$ (red) and $\alpha_{yy}^{\text{mm}}\omega Z_0^{-1}$ (blue), (b) $\alpha_{yx}^{\text{ee}}\omega Z_0$ (black) and $\alpha_{xy}^{\text{mm}}\omega Z_0^{-1}$ (pink), (c) $\alpha_{xx}^{\text{me}}\omega$ (gold) and $\alpha_{yy}^{\text{em}}\omega$ (cyan), (d) $\alpha_{xy}^{\text{em}}\omega$ (green) and $\alpha_{yx}^{\text{me}}\omega$ (purple) of the composite MCh metasurface with $m = \pm 0.3$. Magnetic dipole represented by $\alpha_{yy}^{\text{mm}}\omega Z_0^{-1}$ in Fig. 8(a) shows a sharp resonant feature at 12 GHz compared to the ordinary MCh metasurfaces shown in Figs. 5(a). It can be clearly confirmed that magneto-optical effect is eliminated as in Fig. 8(b) and optical activity is cancelled as in Fig. 8(c). Contrastingly

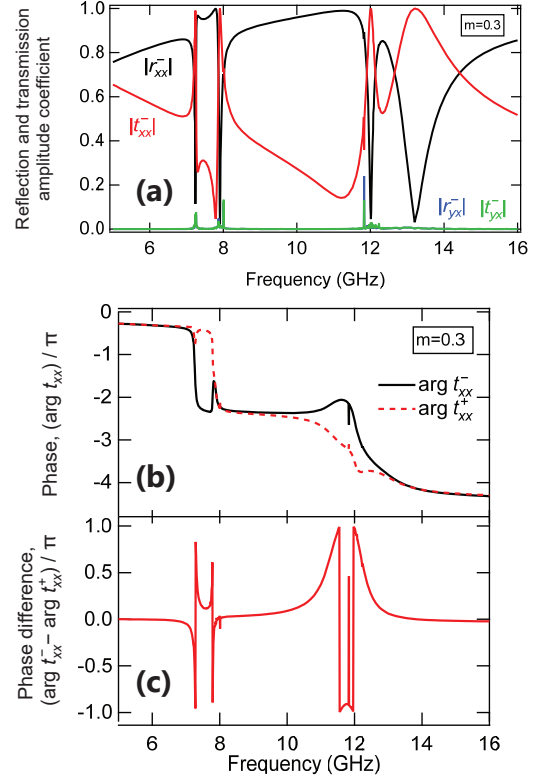


FIG. 7. (a) Calculated spectra of $|r_{xx}^-|$ (black), $|t_{xx}^-|$ (red), $|r_{yx}^-|$ (blue), and $|t_{yx}^-|$ (green) between 4 to 16 GHz of composite MCh metasurface of ordinary MCh metasurfaces with $m = +0.3$ and contraposition MCh metasurfaces with $m = -0.3$. (b) Calculated spectra of $(\arg t_{xx}^-)/\pi$ (black solid) and $(\arg t_{xx}^+)/\pi$ (red dashed), and (c) $(\arg t_{xx}^- - \arg t_{xx}^+)/\pi$ between 4 to 16 GHz for composite MCh metasurface.

and most strikingly, Fig. 8(d) demonstrates that moving bianisotropy survives. Moving bianisotropy at 12 GHz is much more enhanced than that at 7.5 GHz.

In Fig. 8(a), we notice at 12 GHz that $\text{Re}[\alpha_{xx}^{\text{ee}}\omega Z_0] = \text{Re}[\alpha_{yy}^{\text{mm}}\omega Z_0^{-1}]$ and $\text{Im}[\alpha_{xx}^{\text{ee}}\omega Z_0] = \text{Im}[\alpha_{yy}^{\text{mm}}\omega Z_0^{-1}]$, corresponding to the Kerker condition [47]. This results in impedance matching, giving rise to perfect transmission and no reflection. Indeed in transmission and reflection amplitude spectra shown in Fig. 7(a), perfect transmission and no reflection are achieved at 12 GHz. In Fig. 8(d), we observe that $|\alpha_{xy}^{\text{em}}\omega|$ is maximized, i.e., $|\alpha_{xy}^{\text{em}}\omega| = 1$, at 12 GHz. The maximized $|\alpha_{xy}^{\text{em}}\omega| = 1$ derives automatically both perfect transparency and phase difference of π as proved in the following. In the moving medium, i.e., $\hat{\alpha}_{xy}^{\text{em}} = \hat{\alpha}_{yx}^{\text{me}}$, Eq. (14) is written as

$$\tilde{t}_{xx}^+ - \tilde{t}_{xx}^- = -2j\omega\hat{\alpha}_{xy}^{\text{em}}. \quad (16)$$

Absolute value of Eq. (16) is

$$2|\omega\hat{\alpha}_{xy}^{\text{em}}| = |\tilde{t}_{xx}^+ - \tilde{t}_{xx}^-| \leq |\tilde{t}_{xx}^+| + |\tilde{t}_{xx}^-| \leq 2. \quad (17)$$

Equation (17) demonstrates that the maximum value $|\alpha_{xy}^{\text{em}}\omega| = 1$ is achieved when $\tilde{t}_{xx}^+ = -\tilde{t}_{xx}^-$ and $|\tilde{t}_{xx}^\pm| = 1$.

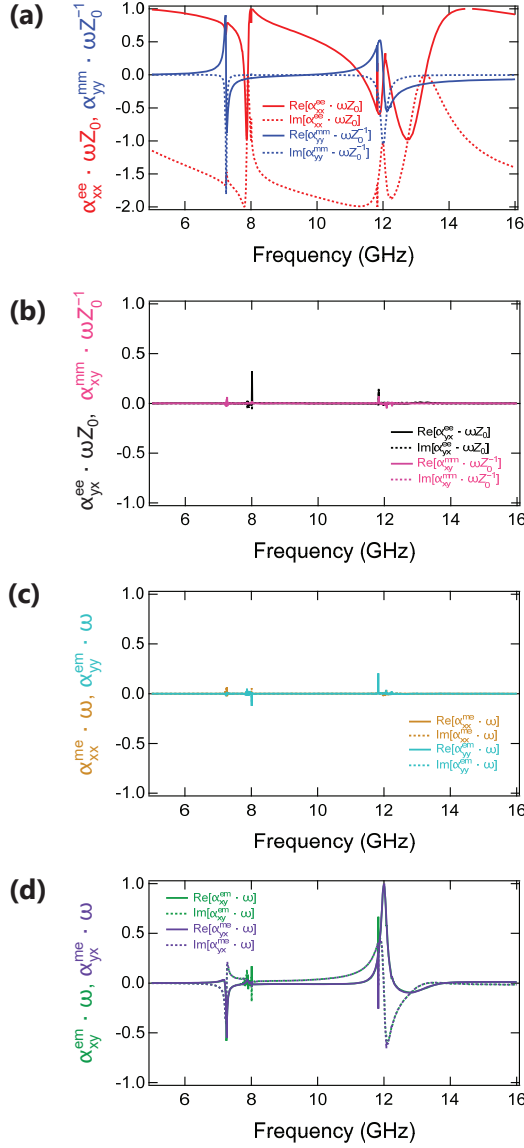


FIG. 8. Effective polarizabilities of composite MCh metasurfaces evaluated from numerical simulation. Frequency versus extracted (a) $\alpha_{xx}^{ee}\omega Z_0$ (red) and $\alpha_{yy}^{mm}\omega Z_0^{-1}$ (blue), (b) $\alpha_{yx}^{ee}\omega Z_0$ (black) and $\alpha_{xy}^{mm}\omega Z_0^{-1}$ (pink), (c) $\alpha_{xx}^{me}\omega$ (gold) and $\alpha_{yy}^{em}\omega$ (cyan), (d) $\alpha_{xy}^{em}\omega$ (green) and $\alpha_{yx}^{me}\omega$ (purple) of the composite metasurfaces consisting of ordinary MCh metasurfaces with $m = +0.3$ and contraposition MCh metasurfaces with $m = -0.3$. Solid and dotted lines correspond to real and imaginary parts, respectively.

Indeed, Fig. 7(c) shows $(\arg t_{xx}^- - \arg t_{xx}^+)/\pi = 1$ at 12 GHz.

The effective polarizability tensor $|\alpha_{xy}^{em}\omega|$, transmission coefficient $|t_{xx}^-|$, and phase difference $(\arg t_{xx}^- - \arg t_{xx}^+)/\pi$ at 12.0 GHz are calculated and evaluated with an increase in parameter m related to magnetization from $m = 0$ to 0.5. Figure 9 highlights $|\alpha_{xy}^{em}\omega|$ (blue, left axis), $|t_{xx}^-|$ (red, left axis), and $(\arg t_{xx}^- - \arg t_{xx}^+)/\pi$ (black, right axis) at 12.0 GHz plotted as a function of

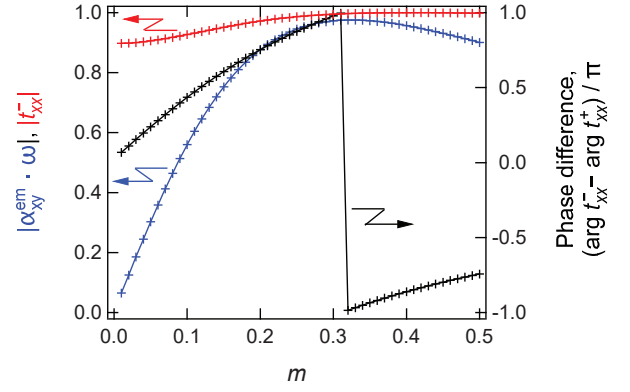


FIG. 9. $|\alpha_{xy}^{em}\omega|$ (blue, left axis), $|t_{xx}^-|$ (red, left axis), and $(\arg t_{xx}^- - \arg t_{xx}^+)/\pi$ (black, right axis) at 12.0 GHz are plotted as a function of m from 0 to 0.5.

m . In Fig. 9, $m = 0.31$ brings about maximum value of $|\alpha_{xy}^{em}\omega| = 0.975$, which is accompanied by $(\arg t_{xx}^- - \arg t_{xx}^+)/\pi = 1.0$ and $|t_{xx}^-| = 1.0$. In this way, the ideal gyrator for arbitrary polarizations is realized using composite metasurface with ordinary and contraposition MCh metasurfaces.

CONCLUSION

Effective polarizability tensor is numerically evaluated to study bianisotropy in MCh metasurfaces. Ordinary MCh metasurface consisting of the double Z-type gammadions for chirality with perpendicularly magnetized substrate shows the non-reciprocal moving-type bianisotropy as well as reciprocal chiral-type bianisotropy and non-reciprocal magneto-optical effect. The chiral-type bianisotropy and magneto-optical effect are eliminated by the combination of ordinary MCh metasurfaces and contraposition MCh metasurfaces having inverse-Z-type gammadion and oppositely magnetized substrates, leading to realization of pure-moving electromagnetic media. The pure moving electromagnetic media demonstrate perfect transmission with phase difference of π , which is a key to embody an ideal gyrator for arbitrary spatial and polarization modes for isolator, circulator, non-reciprocal holography, and two-wavelength lasing. Furthermore, the pure moving media is relevant in an analogy with a hypothetical particle called dyon and in interplay between physics and algebraic geometry in Fresnel-Kummer surfaces.

ACKNOWLEDGMENT

The authors are grateful to Y. Tamayama and T. Ueda for fruitful discussions and comments. H. Kurosawa is also acknowledged for instructing the numerical calcu-

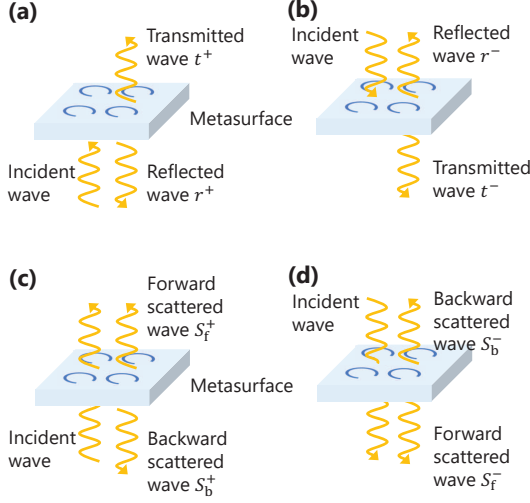


FIG. 10. (a) Transmitted wave t^+ and reflected wave r^+ by incident wave in positive direction (+). (b) Transmitted wave t^- and reflected wave r^- by incident wave in negative direction (-). (c) Redrawn of (a) using forward scattered wave S_f^+ and backward scattered wave S_b^+ . (d) Redrawn of (b) using forward scattered wave S_f^- and backward scattered wave S_b^- .

lation prior to this work. This work is financially supported by KAKENHI (23K13621) and JST-CREST (JP-MJCR2102).

Principle of parameter retrieving

In this Appendix, we provide physical insights into the parameter retrieving given by Eqs. (2) to (9). For sake of simplicity, we consider the case without polarization rotation $t_{xy}^\pm = t_{yx}^\pm = r_{xy}^\pm = r_{yx}^\pm = 0$. Moreover, we simplify as $t^\pm = t_{xx}^\pm$ and $r^\pm = r_{xx}^\pm$. Figures 10(a) and 10(b) illustrate electromagnetic responses by incident waves propagating in the positive and negative direction, respectively. Electromagnetic waves in Figs. 10(a) and 10(b) can be regarded as superpositions of incident waves and scattered waves S_l^\pm ($l = f, b$) radiated by electric and/or magnetic responses of the metasurface as shown in Figs. 10(c) and 10(d). The superscript, \pm , represents the direction of the incident waves, and S_f^\pm (S_b^\pm) represents the scattered waves propagating forward (backward) with respect to the incident waves. Comparing Figs. 10(a) (b) and (c) (d), we obtain

$$t^\pm = 1 + S_f^\pm, \quad (18)$$

$$r^\pm = S_b^\pm. \quad (19)$$

On the metasurface, electric and magnetic fields co-exist for one-way propagating waves. Nevertheless, either the electric fields or magnetic fields can be zero by

destructive interference between plane waves with opposite propagation directions, which form standing waves. For example, when electromagnetic waves with in-phase electric fields propagating in opposite directions are incident on the metasurface, the electric fields are constructively interfered, and the magnetic fields are completely suppressed. As a result, only electric fields induce electric dipole moment P and magnetic dipole moment M on the metasurfaces, resulting in $P = \hat{\alpha}^{ee} E^{\text{inc}}$ and $M = \hat{\alpha}^{me} E^{\text{inc}}$. Total scattered waves can be obtained by adding the scattered waves in Figs. 10(c) and 10(d):

$$S^\uparrow = S_f^+ + S_b^- = t^+ + r^- - 1, \quad (20)$$

$$S^\downarrow = S_b^+ + S_f^- = t^- + r^+ - 1, \quad (21)$$

where S^\uparrow (S^\downarrow) represents the scattered waves propagating in upward (downward) direction. The electric dipole moment P excited on the metasurface radiates in-phase electric fields whereas the magnetic dipole moment M radiates out-of-phase electric fields (or in-phase magnetic fields). In other words, a symmetric component of S^\uparrow and S^\downarrow gives electric dipole radiation, while an anti-symmetric component of S^\uparrow and S^\downarrow gives magnetic dipole radiation. Therefore, we obtain

$$\hat{\alpha}^{ee} \propto S^\uparrow + S^\downarrow = t^+ + t^- + r^+ + r^- - 2, \quad (22)$$

$$\hat{\alpha}^{me} \propto S^\uparrow - S^\downarrow = t^+ - t^- - r^+ + r^-. \quad (23)$$

Equation (22) corresponds to Eq. (2) while Eq. (23) corresponds to Eq. (5).

Contrastingly, magnetic response $P = \hat{\alpha}^{em} H^{\text{inc}}$ and $M = \hat{\alpha}^{mm} H^{\text{inc}}$ can be obtained by incident electromagnetic waves propagating in opposite directions with out-of-phase electric fields. In this case, total scattered waves can be derived by subtracting the field in Fig. 10(d) from that in Fig. 10(c):

$$S^\uparrow = S_f^+ - S_b^- = t^+ - r^- - 1, \quad (24)$$

$$S^\downarrow = S_b^+ - S_f^- = -t^- + r^+ + 1. \quad (25)$$

A symmetric component of Eqs. (24) and (25) gives electric dipole radiation, whereas an anti-symmetric component gives magnetic dipole radiation. Therefore, we acquire

$$\hat{\alpha}^{em} \propto S^\uparrow + S^\downarrow = t^+ - t^- + r^+ - r^-, \quad (26)$$

$$\hat{\alpha}^{mm} \propto S^\uparrow - S^\downarrow = t^+ + t^- - r^+ - r^- - 2. \quad (27)$$

Equation (26) corresponds to Eq. (4) whereas Eq. (27) correspond to Eq. (3).

* Email address:tkodama@tohoku.ac.jp

† Email address:tomita@tohoku.ac.jp

- [1] L. D. Landau, E. M. Lifshitz, and L. P. Pitaevski, *Electrodynamics of Continuous Media* (2nd edition) (Butterworth-Heinemann, Oxford, 1984).
- [2] J. A. Kong, *Electromagnetic Wave Theory* (EMW Publishing, Cambridge, 2005).
- [3] C. Simovski and S. Tretyakov, *An introduction to Metamaterials and Nanophotonics* (Cambridge University Press, 2020).
- [4] V. S. Asadchy, A. Díaz-Rubio, and S. A. Tretyakov, *Bianisotropic Metasurfaces: Physics and Applications*, *Nanophotonics*, 7, 1069 (2018).
- [5] S. Toyoda, N. Abe, S. Kimura, Y. H. Matsuda, T. Nomura, A. Ikeda, S. Takeyama, and T. Arima, *One-Way Transparency of Light in Multiferroic CuB_2O_4* , *Phys. Rev. Lett.* 115, 267207 (2015).
- [6] A. M. Kuzmenko, V. Dziom, A. Shuvaev, Anna Pimenov, M. Schiebl, A. A. Mukhin, V. Yu. Ivanov, I. A. Gudim, L. N. Bezmaternykh, and A. Pimenov, *Large directional optical anisotropy in multiferroic ferrobamate*, *Phys. Rev. B* 92, 184409 (2015).
- [7] M. Fiebig, T. Lottermoser, D. Meier and M. Trassin, *The evolution of multiferroics*, *Nature Reviews Materials* 1, 16046 (2016).
- [8] X. Chen, B.-I. Wu, J. A. Kong, and T. M. Grzegorzczak, *Retrieval of the effective constitutive parameters of bianisotropic metamaterials*, *Phys. Rev. E* 71, 046610 (2005).
- [9] N. Kida, T. Yamada, M. Konoto, Y. Okimoto, T. Arima, K. Koike, H. Akoh, and Y. Tokura, *Optical Magnetoelectric Effect in a Submicron Patterned Magnet*, *Phys. Rev. Lett.* 94, 077205 (2005).
- [10] E. Plum, V. A. Fedotov, and N. I. Zheludev, *Extrinsic electromagnetic chirality in metamaterials*, *J. Opt. A: Pure Appl. Opt.* 11 074009 (2009).
- [11] Z. Li, K. Aydin, and E. Ozbay, *Determination of the effective constitutive parameters of bianisotropic metamaterials from reflection and transmission coefficients*, *Phys. Rev. E* 79, 026610 (2009).
- [12] T. Niemi, A. O. Karilainen, and S. A. Tretyakov, *Synthesis of Polarization Transformers*, *IEEE Trans. Antennas Propag.* 61, 3102 (2013).
- [13] C. Pfeiffer, and A. Grbic, *Bianisotropic Metasurfaces for Optimal Polarization Control: Analysis and Synthesis*, *Phys. Rev. Applied* 2, 044011 (2014).
- [14] C. Pfeiffer, C. Zhang, V. Ray, L. Jay Guo, and A. Grbic, *High Performance Bianisotropic Metasurfaces: Asymmetric Transmission of Light*, *Phys. Rev. Lett.* 113, 023902 (2014).
- [15] M. Odit, P. Kapitanova, P. Belov, R. Alaee, C. Rockstuhl, and Y. S. Kivshar, *Experimental realisation of all-dielectric bianisotropic metasurfaces*, *Appl. Phys. Lett.* 108, 221903 (2016).
- [16] G. Lavigne and C. Caloz, *Generalized Brewster effect using bianisotropic metasurfaces*, *Opt. Expr.* 29, 11361 (2021).
- [17] M. P. Groenewege, *Mol. Phys.* 5, 541 (1962).
- [18] D. L. Portigal and E. Burstein, *J. Phys. Chem. Solids* 32, 603 (1971).
- [19] N. B. Baranova, Yu. V. Bogdanov, and B. Ya. Zeldovich, *Opt. Commun.* 22, 243 (1977).
- [20] V. A. Markelov, M. A. Novikov, and A. A. Turkin, *Zh. Pis'ma Eksp. Teor. Fiz.* 25, 404 (1977) [*JETP Lett.* 25, 378 (1977).]
- [21] N. B. Baranova and B. Ya. Zeldovich, *Mol. Phys.* 38, 1085 (1979).
- [22] G. Wagnière and A. Meier, *Chem. Phys. Lett.* 93, 78 (1982).
- [23] G. Wagnière, *Chem. Phys. Lett.* 110, 546 (1984).
- [24] L. D. Barron and J. Vrbancich, *Mol. Phys.* 51, 715 (1984).
- [25] G. L. J. A. Rikken and E. Raupach, *Nature*, 390, 493 (1997).
- [26] P. Kleindienst and G. H. Wagnière, *Chem. Phys. Lett.* 288, 89 (1998).
- [27] G. L. J. A. Rikken and E. Raupach, *Pure and cascaded magnetochiral anisotropy in optical absorption*, *Phys. Rev. E* 58, 5081 (1998).
- [28] M. Vallet, R. Ghosh, A. Le Floch, T. Ruchon, F. Bretenaker, and J.-Y. Thépot, *Observation of Magnetochiral Birefringence*, *Phys. Rev. Lett.* 87, 183003 (2001).
- [29] C. Train, R. Gheorghe, V. Krstic, L.-M. Chamoreau, N. S. Ovanesyan, G. L. J. A. Rikken, M. Gruselle, and M. Verdaguer, *Strong magneto-chiral dichroism in enantiopure chiral ferromagnets*, *Nature Mater.* 7, 729-734 (2008).
- [30] S. Tomita, K. Sawada, A. Porokhnyuk, and T. Ueda, *Direct Observation of Magnetochiral Effects through a Single Metamolecule in Microwave Regions*, *Phys. Rev. Lett.* 113, 235501 (2014).
- [31] S. Tomita, H. Kurosawa, T. Ueda, and K. Sawada, *Metamaterials with magnetism and chirality*, *J. Phys. D: Appl. Phys.* 51, 083001 (2018).
- [32] M. Atzori, G. L. J. A. Rikken, and C. Train, *Magneto-Chiral Dichroism: A Playground for Molecular Chemists*, *Chem. Eur. J.* 2020, 26, 9784 (2020).
- [33] J. M. Caridad, C. Tserkezis, J. E. Santos, P. Plochocka, M. Venkatesan, J. M. D. Coey, N. Asger Mortensen, G. L. J. A. Rikken, and V. Krstić, *Detection of the Faraday Chiral Anisotropy*, *Phys. Rev. Lett.* 126, 177401 (2021).
- [34] M. S. Mirmoosa, Y. Ra'di, V. S. Asadchy, C. R. Simovski, and S. A. Tretyakov, *Polarizabilities of Nonreciprocal Bianisotropic Particles*, *Phys. Rev. Appl.* 1, 034005 (2014).
- [35] R. Alaee, M. Albooyeh, M. Yazdi, N. Komjani, C. Simovski, F. Lederer, and C. Rockstuhl, *Magnetoelectric coupling in nonidentical plasmonic nanoparticles: Theory and applications*, *Phys. Rev. B* 91, 115119 (2015).
- [36] M. Yazdi and N. Komjani, *Polarizability Calculation of Arbitrary Individual Scatterers, Scatterers in Arrays, and Substrated Scatterers*, *J. Opt. Soc. Am. B* 33, 491 (2016).
- [37] D. M. Pozar, *Microwave Engineering*, 3rd. Ed. (Wiley, 2005).
- [38] D. R. Smith, J. Gollub, J. J. Mock, W. J. Padilla, D. Schurig, *Calculation and measurement of bianisotropy in a split ring resonator metamaterial*, *J. Appl. Phys.* 100, 024507 (2006).
- [39] C. É. Kriegler, M. S. Rill, S. Linden, and M. Wegener, *Bianisotropic Photonic Metamaterials*, *IEEE Journal of Selected Topics in Quantum Electronics* 16, 367 (2010).
- [40] W. Yang, J. Qin, J. Long, W. Yan, Y. Yang, C. Li, E. Li, J. Hu, L. Deng, Q. Du, and L. Bi, *A self-biased non-reciprocal magnetic metasurface for bidirectional phase modulation*, *Nat. Electron* 6, 225-234 (2023).
- [41] K. Sawada and N. Nagaosa, *Optical Magnetoelectric Effect in Multiferroic Materials: Evidence for a Lorentz Force Acting on a Ray of Light*, *Phys. Rev. Lett.* 95, 237402 (2005).
- [42] D. I. Khomskii, *Magnetic monopoles and unusual dynamics of magnetoelectrics*, *Nature Commun.* 5,4793 (2014).

- [43] R. W. H. T Hudson, Kummer's Quartic Surface, (the University Press, Cambridge, 1905).
- [44] A. Favaro and F. W. Hehl, Light propagation in local and linear media: Fresnel-Kummer wave surfaces with 16 singular points, Phys. Rev. A 93, 013844 (2016).
- [45] T.T. Kim, S. S. Oh, H.-S. Park, R. Zhao, S.-H. Kim, W. Choi, B. Min, and O. Hess, Optical Activity Enhanced by Strong Inter-Molecular Coupling in Planar Chiral Metamaterials, Scientific Reports 4, 5864 (2014).
- [46] B. D. Tellegen, The gyrator, a new electric network element, Philips Res Rep 3, 81-101, (1948).
- [47] M. Kerker, D.-S. Wang, and C. Giles, J. Opt. Soc. Am. A 73, 765 (1983).